Analysis of Factors Affecting Activity of Non-Precious Metal ORR Catalysts for PEM Fuel Cells

A Bachelors of Science Thesis

Prepared in Accordance to Requirements for

Graduation with Distinction in Chemical and Biomolecular Engineering

By

Jesaiah Christopher King

* * * *

The Ohio State University

2013

Dissertation Committee:

Professor Umit S. Ozkan, Advisor

Professor Aravind Asthagiri

Abstract

Fuel cells are currently the focus of much interest and research. They are also an integral part of the Hydrogen Economy and show much potential for environmentally-friendly mobile and stationary power generation. Of the types of fuel cells, the proton exchange membrane fuel cell (PEMFC) has shown traits desirable for vehicular application including short start-up times and lower operating temperatures. One of the major hindrances to commercialization of PEMFCs is that platinum is used for the cathode. This is an issue because of platinum's limited availability and cost, both of which would not work well with economies of scale. These limitations have encouraged research into non-precious metal catalysts (NPMC) for PEMFCs.

This project was concerned with the development of NPMC for PEMFCs and was focused on improving catalytic activity so that NPMCs can operate comparably to platinum. Several NPMCs were synthesized for this project. The multistep-preparation process began with wetness impregnation followed by ballmilling, heat treatment in an inert gas, and ended with heat treatment in a reactive gas. The effects of varying the non-precious metal precursor used in wetness impregnation, inert gas, reactive gas, and reactive-gas heat-treatment duration will be explored. Electrochemical experiments to determine the activity of these catalysts were completed, and it was found that the second heat treatment improved catalytic activity. Statistical analysis will also be used to qualitatively determine the influence of preparation parameters on catalytic performance.

This project aimed to examine the feasibility of using statistical modeling for estimation of the influence of preparation parameters on catalytic activity of NPMC towards the ORR with the long-term goal of optimization of catalytic activity and eventual marketability of NPMC catalysts.

Dedication

To my family and friends who have put up with not seeing me for long stretches of time so that I could complete this work and my undergraduate education.

To Dr. Matthew Stoltzfus who inspired me to pursue research.

To Jesus Christ for giving me life and truth.

Acknowledgements

I gratefully acknowledge the teaching, guidance, and camaraderie I have received in the laboratory from all the past and present Heterogeneous Catalysis Research Group members.

It would be impossible for me not to thank the former and present graduate students I've known for helping me acclimate to the idea and lifestyle of graduate school. Thank you Dr. Preshit Gawade, Dr. Ilgaz Soykal, Dr. Elizabeth Biddenger, Dr. Dieter von Deak, Dr. Hyunkyu Choi, Deepika Singh Jha, Anshuman Fuller, Hyuntae Sohn, Sreshtha Majumdar, Katja Binkley, Kuldeep Mamtani, and Gokhan Celik.

I especially wish to thank Dr. Elizabeth Biddenger, Dr. Dieter von Deak, Dr. Juan Tian, and Deepika Singh Jha for all of the advice, wisdom, and guidance they've imparted to me while being part of the PEM Team. I've greatly enjoyed working with and getting to know each one of you.

None of this research would have been possible without Dr. Umit Ozakn. Her wisdom, advice, and guidance have been invaluable. I thank her much for letting me become a part of her family.

Table of Contents

List of Figures

List of Tables

Introduction

Fuel cells are currently the focus of much interest and research. They are also an integral part of the Hydrogen Economy and show much potential for environmentally-friendly mobile and stationary power generation.

There are five main types of fuel cells, each named after the electrolyte it uses: proton exchange (or polymer electrolyte) membrane (PEM), alkaline, phosphoric acid, molten carbonate, and solid oxide. PEM fuel cells (PEMFC) use a polymeric membrane that conducts protons, normally Nafion. Alkaline fuel cells (AFC) use basic solution, typically potassium hydroxide. Phosphoric acid fuel cells (PAFC) use phosphoric acid in a matrix. Molten carbonate fuel cells (MCFC) use a molten metal (lithium, sodium, magnesium) carbonate. Solid oxide fuel cells (SOFC) use yttria-stabilized zirconia.[1, 2] Figure 1 gives an overview of these fuel cells.

U.S. DEPARTMENT OF ENERGY | Energy Efficiency & Renewable Energy

FUEL CELL TECHNOLOGIES PROGRAM

Comparison of Fuel Cell Technologies

Fuel Cell Type	Common Electrolyte	Operating Temperature	Typical Stack Size	Efficiency	Applications	Advantages	Disadvantages
Polymer Electrolyte Membrane (PEM)	Perfluoro sulfonic acid	50-100°C 122-212° typically 80°C	< 1kW–100kW	60% transportation 35% stationary	• Backup power • Portable power • Distributed generation • Transporation • Specialty vehicles	• Solid electrolyte reduces corrosion & electrolyte management problems • Low temperature • Quick start-up	• Expensive catalysts • Sensitive to fuel impurities • Low temperature waste heat
Alkaline (AFC)	Aqueous solution of potassium hydroxide soaked in a matrix	90-100°C 194-212°F	10–100 kW	60%	• Military • Space	• Cathode reaction faster in alkaline electrolyte, leads to high performance • Low cost components	• Sensitive to CO_2 in fuel and air • Electrolyte management
Phosphoric Acid (PAFC)	Phosphoric acid soaked in a matrix	150-200°C 302-392°F	400 kW 100 kW module	40%	• Distributed generation	• Higher temperature enables CHP • Increased tolerance to fuel impurities	• Pt catalyst • Long start up time • Low current and power
Molten Carbonate (MCFC)	Solution of lithium, sodium, and/or potassium carbonates, soaked in a matrix	600-700°C 1112-1292°F	300 kW-3 MW 300 kW module	45-50%	• Electric utility • Distributed generation	• High efficiency • Fuel flexibility • Can use a variety of catalysts • Suitable for CHP	• High temperature corrosion and breakdown of cell components • Long start up time • Low power density
Solid Oxide (SOFC)	Yttria stabilized zirconia	700-1000°C 1202-1832°F	1 kW–2 MW	60%	• Auxiliary power • Electric utility • Distributed generation	• High efficiency • Fuel flexibility • Can use a variety of catalysts • Solid electrolyte • Suitable for CHP & CHHP • Hybrid/GT cycle	• High temperature corrosion and breakdown of cell components • High temperature operation requires long start up time and limits

Figure 1. Comparison of Fuel Cells. Reproduced from[2]

While each kind of fuel cell has its own advantages and disadvantages, the US Department of Energy has decided that the PEMFC is the best candidate for use in vehicular transportation, primarily due to lower operating temperatures and simpler design possibilities due to the absence of a corrosive liquid electrolyte. The benefits of a viable, vehicular PEMFC compared to the internal combustion engine are improved efficiency, greater energy independence, and cleaner emissions.[3]

Fuel cells generate power by separating two electrochemical reactions and through using an electrically insulative electrolyte that allows the transfer of ions to

maintain neutrality.[1] Figure 2 is an example of the membrane electrode assembly (MEA) of a proton exchange membrane (PEM) fuel cell. In a PEM fuel cell hydrogen flows to a gas diffusion layer (GDL) where it disperses onto the anode. The hydrogen is then split into protons and electrons. The protons travel through the membrane to the cathode and the electrons generate power by travelling through a circuit on their way to the cathode. Concurrently, oxygen travels to and disperses through another GDL onto the cathode, where it reacts with the protons and electrons to form water. The water and any unreacted gas then disperse through and out of the GDL and leave the MEA.

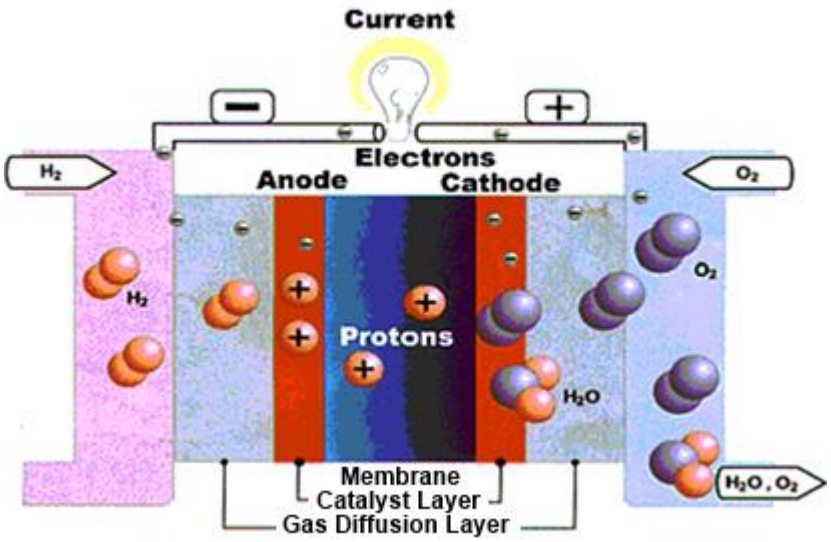

Figure 2. MEA of a PEM Fuel Cell. Adapted from[4]

While the PEMFC shows promise for vehicular application, several roadblocks have kept it from viability: the cathode catalyst for the oxygen-reduction reaction (ORR),

hydrogen usage, and logistics. The only viable cathode catalyst for PEMFC is platinum or an alloy thereof. While great strides have been made with regards to platinum activity,[5] its availability is uncertain and its price volatile.[6, 7] Moreover, before purification, the vast majority of hydrogen produced contains carbon monoxide and sulfur, both of which are known poisons of platinum.[3, 8-11] Therefore, to use hydrogen and avoid significant deactivation of the platinum catalyst at the anode, the hydrogen must be very pure or another technology would need to demonstrate that it could meet the expected demands of quantity and purity. Either way involves significant cost. Additional cost is accrued by the necessity of high pressures to achieve the desired activity and volume requirements.[3, 12] As if the cost of using hydrogen was not trouble enough, the public is fearful of using hydrogen as a fuel, perhaps due to negative association with the Hindenburg incident.[9, 13, 14] Finally, the inputs of economic analyses of PEMFC prepared for the U.S. Department of Energy are from disparate companies and an economically viable PEMFC has yet to be demonstrated.[12]

The expense of platinum has driven research for alternative non-precious metal catalysts (NPMCs) for use in PEMFC. NPMC have been synthesized using abundant and inexpensive precursors and have demonstrated qualities that are desirable for use in PEMFC. Although less expensive, NPMC have not yet reached activity and stability comparable to platinum. Nonetheless, NPMC could still be a viable catalyst since higher loadings can be used to compensate for lower activity. Ultimately, whether NPMC are

used in PEMFC or not will be determined by the achievable power density within desired loading requirements.[15, 16]

This project is concerned with the development of NPMC for PEMFC and is focused on improving catalytic activity of a subclass of NPMC denoted Fe/N/C so that they could eventually operate comparably to platinum. The subclass Fe/N/C will be discussed in greater detail in the literature review.

Several Fe/N/C catalysts were synthesized and electrochemically tested for this project. The effects of preparation parameters were statistically analyzed with the intent of determining which parameters significantly affect activity. This project aimed to examine the feasibility of using statistical modeling for estimation of the influence of preparation parameters on catalytic activity of NPMC towards the ORR with the long-term goal of optimization of catalytic activity and eventual marketability of NPMC catalysts. A first-order experimental design was used and yielded parameter estimates of -16.6 mv, 16.6 mV, -20.6 mV, and 20.6 mV for Ketjen black, Black pearls, acetonitrile, and ammonia. Although the model was significant, it did not fit the data well.

Literature Review

NPMC for fuel cells were pioneered almost 50 years ago by Jasinski using cobalt phthalocyanine (CoPc) in an alkaline solution.[17] Subsequently, NPMC have undergone three major stages of development and comprise materials ranging from heteropoly acids to carbon nanotubes.[18]The first NPMC for fuel cells were chelated-transition-metal macrocycles whose use as a catalyst for fuel cells was inspired by heme and the usage of metal phthalocyanines in the oxidation of organic molecules.[17, 19] The coordinated-metal centers were reported to form bridged oxygen complexes with the potential for the four electron reduction of oxygen.[20, 21] Although these catalysts were active for ORR, they lacked the stability for use in a fuel cell environment and have been used mainly to investigate the active site and ORR mechanism.[21-23] Moreover, macrocycles can be expensive and thereby defeat the objective of finding inexpensive alternatives to platinum. Examples of macrocyclic compounds are given in Figures 3.

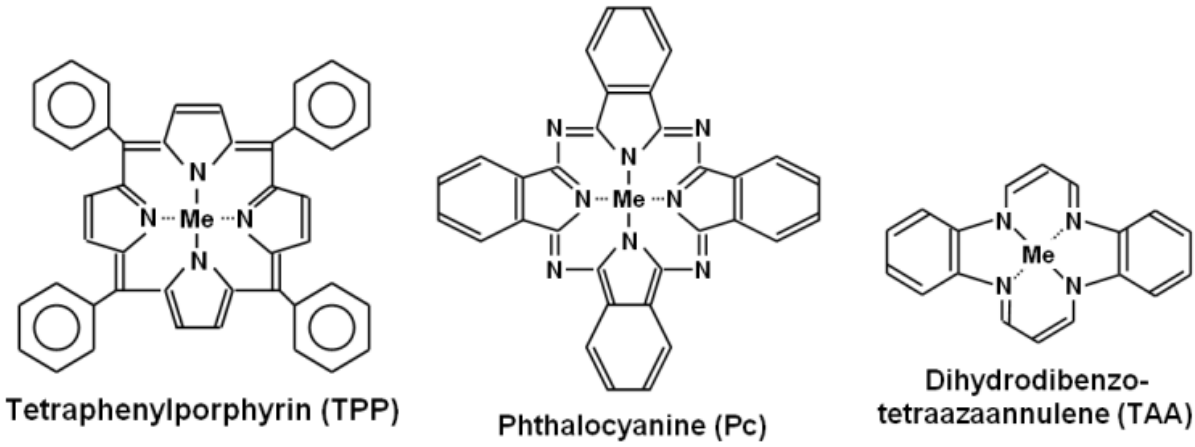

Figure 3. Metal Macrocycles as Reproduced from[24].

The next stage in NPMC development occurred when the aforementioned macrocycles were subjected to a thermal pretreatment. This was found to improve the activity and stability of the NPMC and this improvement was found to depend upon the macrocyclic compound, carbon support, treatment environment (e.g. inert, reductive, etc.), and temperature.[23, 24] There are several schools of thought concerning how the thermal treatment improves activity and stability. van Veen *et al.* proposed that the stability improvement is caused by the fringes of the macrocycle bonding with the carbon support, thereby removing the portion of the macrocycle most susceptible to oxidative attack and that the activity improvement is due to a change in the electron density around the metal ion resulting in a more favorable redox potential.[25] Yeager *et al.* proposed that heat treatment causes the macrocycles to undergo decomposition and produce surface nitrogen species that serve as adsorption sites for the active metal ions.[20, 21] Another view

proposed that the metal was not part of the active site.[26] A significant characteristic of this stage in NPMC development was the ambiguity of the active site, which was inherited by the third and current stage in development.

In 1989, Gupta *et al.* used separate transition metal and nitrogen sources to create NPMC with activity comparable to traditional NPMC catalysts in alkaline and acidic media.[27] This demonstrated that the metal need not be coordinated with nitrogen prior to heat treatment to obtain active ORR catalysts. Since then numerous combinations of precursors and treatment conditions have been reported in the literature. The general consensus is that an active ORR catalyst requires: (1) a transition metal - thus far Fe and Co have produced the most active catalysts, (2) a source of nitrogen, (3) a carbon source, and (4) an activation step, which is typically thermal.[18, 28-31]

As mentioned in the introduction, the subclass of NPMC titled Fe/N/C will be discussed. The literature describes varied methods of NPMC preparation and testing, which has led to the proposition that there are two probable types of active sites in NPMC catalyst that are prepared with a transition metal, carbon, and nitrogen precursors: a nitrogen-chelated transition-metal moiety (M/N/C) and a nitrogen-doped carbon (CN_X).[18, 28-31] The majority of the catalysts mentioned in this literature review could be considered Fe/N/C or Fe/N/C-like, with a proposed active site consisting of a nitrogen-coordinated iron ion as shown in Figures 4 and 5. Wiesener proposed an alternative active site where the metal activates the carbon, but is not part of the active site.[26, 32] Matter *et al.* proposed

a similar, more specific, active site comprised of pyridinic nitrogen located on graphitic edge planes. This material has subsequently been called CN_X.[33] Both CN_X and Fe/N/C require carbon, nitrogen, a transition metal, and high temperature heat treatment in order to be active for the ORR.[18, 28-31] Nonetheless, there are two main differences: the morphology and the role of the metal.

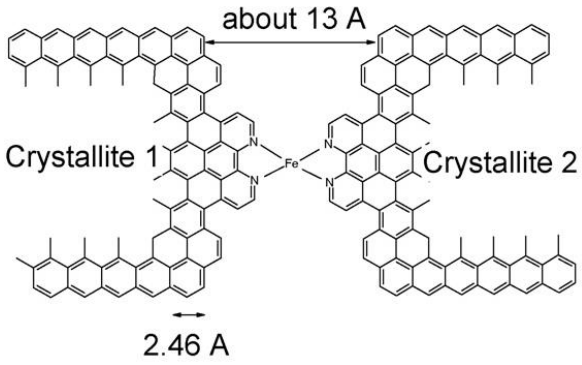

Figure 4. Proposed FeN_{2+2}/C Active Site.[34]

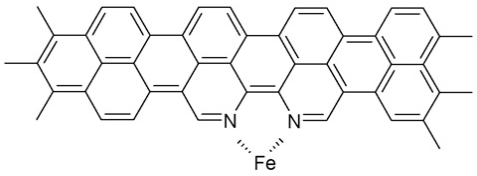

Figure 5. Proposed FeN_2/C Active Site.[34]

The CN_X prepared by Matter *et al.* used an Fe/MgO growth catalyst.[33] Metal particles - especially Fe, Co, and Ni - have long been used to grow carbon nanotubes (CNT) and carbon nanofibers (CNF).[35-40] More recently, metals supported on metal oxides have also shown this ability – including iron supported on magnesia.[41-56] Thus, it is reasonable to assume that the Fe/MgO catalyst used by Matter *et al.* also grew carbon nanofibers. This hypothesis was supported by Mössbauer analysis of the iron.[57] However, the metallic precursors used for Fe/N/C catalysts are typically treated in inert or ammonia.[28] Therefore, since CNT growth using a metal catalyst usually requires a gaseous hydrocarbon or hydrocarbon-like reactant, it is unlikely that the metallic precursor used for Fe/N/C significantly catalyzes the growth of CNT or CNF. Indeed, Lefevre *et al.* used Time-of-Flight Secondary Ion Mass Spectrometry (ToF-SIMS) to show that ORR activity correlated with the observation of an $FeN_2C_4^+$ ion[58], leading them to the conclusion that iron ions are coordinated by pyridinic nitrogens.[58-60] Additionally, when the metal is present above a threshold, the excess metal induces graphitization of nearby carbon and the formation of metal carbides, which are inactive towards the ORR.[61, 62]

The morphological differences between CN_X and Fe/N/C are apparent considering CN_X is composed primarily of nanofibers and the morphology of Fe/N/C is amorphous since it is primarily carbonaceous support. CN_X is nitrogen doped carbon nanofibers that

have mostly assumed stack cup structure as seen in Figure 6, and its activity correlates to the amount of pyridinic nitrogen and graphitic edge planes.[33, 63-65]

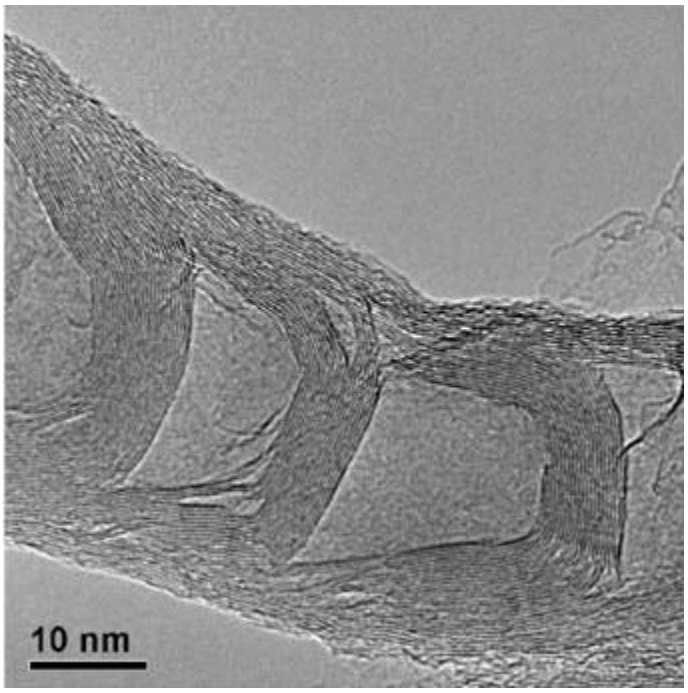

Figure 6. Stacked Cups Grown on Fe/MgO.[33]

The morphology of Fe/N/C is largely determined by the carbon support, which also strongly influences activity towards the ORR.[66, 67] Figure 7 presents an example of Fe/N/C morphology. Correlation between microporous area of pristine carbon support, microporous area created through ammonia etching, degree of disorder of the carbon

support, surface nitrogen content and ORR activity for Fe/N/C catalysts has been observed.[66-76]

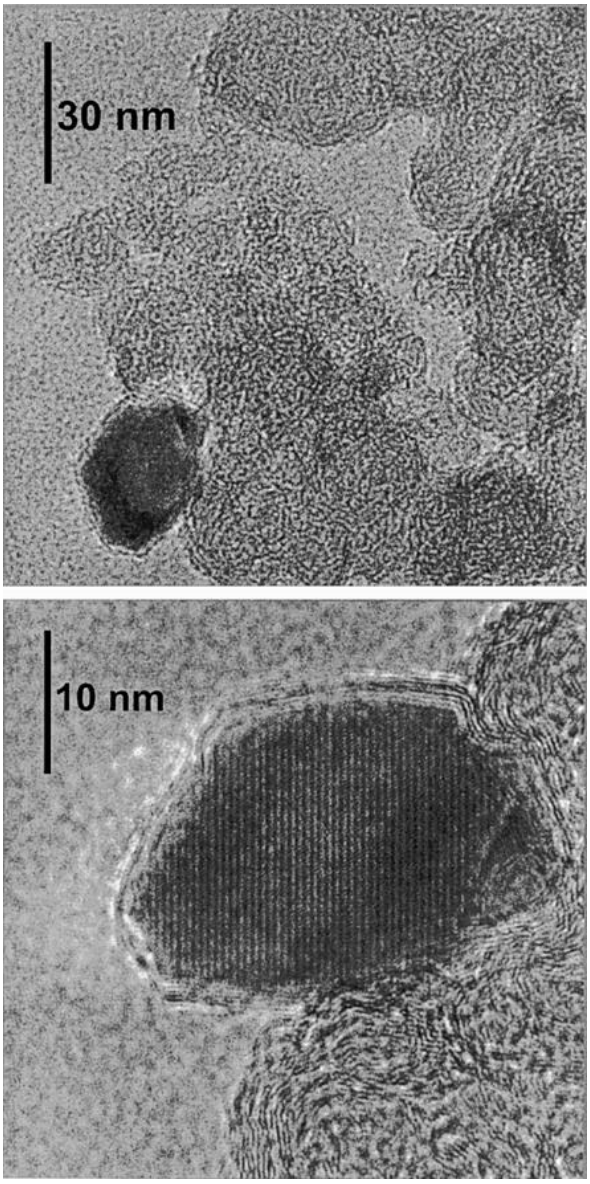

Figure 7. TEM of Fe/N/C.[77]

Experimental Methods

Catalyst Preparation

Catalysts for this project were prepared for three separate sections of experiments: (1) main section, (2) acid-washed section, and (3) third-heat treatment section. Although the preparation varied somewhat for each section, the general experimental procedures were similar and started with a wetness impregnation (WI), followed by ballmilling, an inert pyrolysis, and concluded with a reactive pyrolysis.

Wetness Impregnation (WI)

In the first preparation step a carbon support, iron precursor, and 1,10-phenanthroline (Sigma-Aldrich) were mixed in a 150 mL solution of 2DI-H_2O:1EtOH and heated in a water bath at 60 ˚C until ~50 mL of mixture remained. The WI was then placed into a drying oven at 90 ˚C overnight until the solvent completely evaporated. After the solvent evaporated, the next step was ballmilling. In order to ensure desirable particle size, the dried WI was ground in a mortar and pestle prior to ballmilling.

Ballmilling

The dried WI was placed into a mill jar along with 20 chrome steel balls. The jar and its lid were then placed into a glove bag, which was subsequently purged with nitrogen for at least 30 min. After 30 min, the mill jar was sealed and removed from the glove bag. This step was performed to ensure that there was no oxygen in the sample while it was ballmilling since the oxygen could have reacted with the carbonaceous support and reduced yield. Once the mill jar was purged, it was placed on the ballmill which ran at 200 rpm for 180 min. The ballmilled product was then heat treated in an inert gas.

Inert Pyrolysis

After ballmilling, the carbonaceous product was placed in a quartz boat which was subsequently placed in a quartz tube. The tube was purged with inert that flowed at 150 sccm for at least 30 minutes before pyrolysis. After purging, the furnace was heated from room temperature to 1050 ˚C and once the furnace reached this temperature the quartz boat containing the sample was pushed into the hot zone of the furnace and remained there in an inert atmosphere for 60 min. Afterwards, the quartz tube was removed from the furnace and cooled to room temperature while inert continually flowed

through it. Refer to Figure 8 for a description of the pyrolysis system. After the sample cooled to room temperature, it was removed from the quartz tube and awaited reactive pyrolysis.

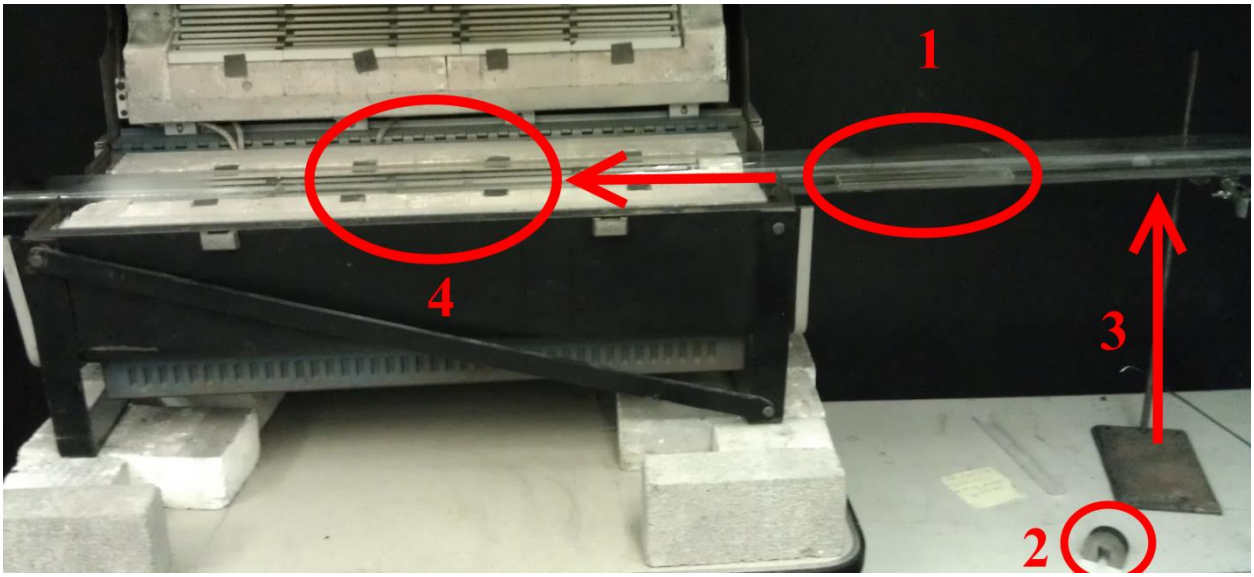

Figure 8. Pyrolysis System.

*Quartz boat (1) and a magnet (2) that is used to move a glass rod (3) such that it pushes the quartz boat into the hot zone (4).

Reactive Pyrolysis

The procedure for the reactive pyrolysis differed for each section and the differences will be described in their respective sections. After inert pyrolysis, the sample was again placed in a quartz boat, which was placed into a quartz tube. The tube was purged with a reactive gas, typically ammonia, flowing at ~150 ccm for at least 30 min

before pyrolysis. After purging the furnace was heated to 950 ˚C, and once the furnace reached that temperature, the quartz boat containing the sample was pushed into the hot zone and typically remained there under ammonia for 20 minutes. Afterwards, the quartz tube was removed from the furnace and cooled to room temperature while inert continually flowed through it. After the sample cooled to room temperature, it was removed from the quartz tube and was electrochemically tested.

Main Section

For the catalysts in this section, the general experimental flow described above was followed with the caveat that the carbon support, acetate/nitrate precursor (both Sigma-Aldrich), inert gas, reactive gas, and reactive gas pyrolysis duration were all varied according to a randomized list generated by the statistical software JMP®.[78] This process will be discussed in greater detail in Appendix A. Table 1 details the precursors and conditions that were varied, while the list of samples and their corresponding precursors and conditions is given in Table 2.

Table 1. List of Precursors and Experimental Conditions.

Carbon Support	Acetate: Nitrate Precursors*	Inert Gas	Reactive Gas	Reactive Gas Pyrolysis Duration (min)
Ketjen Black (KB)	1:0	Argon	Ammonia	5
Black Pearls (BP)	1:1	Nitrogen	Acetonitrile**	20
	0:1			40

* Iron(II) acetate and iron(III) nitrate•nonahydrate were the precursors used and the ratios are on an iron basis.
** Acetonitrile saturated nitrogen.

Table 2. List of Samples and their Corresponding Experimental Conditions.

Sample	Carbon Support	Acetate: Nitrate Precursors	Inert Gas	Reactive Gas	Reactive Pyrolysis Duration (min)
1	BP	1:0	Ar	CH_3CN	40
2	KB	1:1	N_2	NH_3	40
3	KB	1:1	Ar	NH_3	5
4	BP	1:0	Ar	NH_3	5
5	BP	1:0	N_2	NH_3	40
6	BP	0:1	Ar	CH_3CN	5
7	KB	1:0	N_2	CH_3CN	20
8	BP	1:0	N_2	NH_3	5
9	BP	1:1	Ar	CH_3CN	20
10	KB	0:1	N_2	NH_3	5
11	BP	1:1	N_2	NH_3	20
12	BP	0:1	Ar	NH_3	40
13	KB	1:0	Ar	CH_3CN	5
14	KB	1:0	Ar	NH_3	20
15	BP	0:1	N_2	CH_3CN	20
16	KB	1:1	Ar	CH_3CN	40

The procedure used to prepare the main section samples followed the aforementioned description with the caveat that the parameters were varied according to Table 2.

The acetonitrile samples followed a similar procedure as the ammonia samples. The sample was placed into a quartz boat, which was placed into a quartz tube. Nitrogen purged an acetonitrile bubbler for ~30 min before the quartz boat was placed into the quartz tube. Nitrogen bubbled through acetonitrile such that the flow rate of the acetonitrile saturated nitrogen was ~150 sccm. The acetonitrile saturated nitrogen, from now on referred to simply as acetonitrile, purged the quartz tube for at least 30 min before pyrolysis. The furnace was heated to ~900 ˚C, and once this temperature was reached, the furnace was opened and the quartz tube was placed into the furnace. The time at which the furnace reached 900 ˚C again was the reference point used as the start of the reactive pyrolysis. The pyrolysis duration varied according to Table 2. Afterwards,

the quartz tube was removed from the furnace and cooled to room temperature while inert flowed through it. After the sample cooled to room temperature, it was removed from the quartz tube and was electrochemically tested.

Acid Washed Section

For the catalysts in this section, deviations from the outlined procedure will be described. Samples were washed at different stages in the preparation process as described in Table 3.

Table 3. List of Acid Washed Samples and their Experimental Conditions.

Sample	Carbon Support	Acetate: Nitrate Precursors	Inert Gas	Reactive Gas	Reactive Pyrolysis Duration (min)	Acid Wash (HNO_3)
1	KB	1:0	N_2	N/A	N/A	Before inert pyrolysis
2	KB	1:0	N_2	NH_3	5	Before inert pyrolysis
3	KB	1:0	N_2	N/A	N/A	N/A
4	KB	1:0	N_2	N/A	N/A	After inert pyrolysis
5	KB	1:0	N_2	NH_3	5	N/A
6	KB	1:0	N_2	NH_3	5	Between inert and reactive pyrolyses
7	KB	1:0	N_2	NH_3	5	After reactive pyrolysis

The procedure used to prepare the acid washed samples followed the aforementioned description with the caveat that the parameters were varied according to Table 3, the pyrolysis duration was 5 minutes, samples 1 & 2 were acid washed before inert pyrolysis, and sample 6 was washed before reactive pyrolysis.

Acid Wash

250 mL of 1M HNO_3 was prepared by dilution of concentrated HNO_3. The nitric acid was poured into a 500-mL rounded bottom flask (RBF), which was placed into a water bath and heated to 60 ˚C. Once this temperature was reached, the sample was added to the acid, along with a stir bar, and was stirred at 60 ˚C for 60 min. Afterwards, the acidic mixture of the sample and solution was filtered using a Büchner funnel and was rinsed with ~1L of DI-H_2O. The filter cake was then rinsed into a beaker using ~100 mL of DI-H_2O, and was then placed into a drying oven at ~110 ˚C overnight.

Third-Heat Treatment Section

The procedure used to prepare the acid washed samples followed the aforementioned description with the caveat that the parameters were varied according to Table 4, the pyrolysis durations were 20 min, and reactive gas used in the second and third heat treatments were reversed for the two samples as described in Table 4.

Table 4. List of Third-Heat Treatment Samples and their Corresponding Experimental Conditions.

Sample	Carbon Support	Acetate: Nitrate Precursors	Inert Gas	First Reactive Gas	First Reactive Pyrolysis Duration (min)	Second Reactive Gas	Second Reactive Pyrolysis Duration (min)
1	BP	1:0	N_2	NH_3	20	CH_3CN	20
2	BP	1:0	N_2	CH_3CN	20	NH_3	20

Electrochemical Testing

The activity of the samples towards the ORR was measured through cyclic voltammetry (CV) using a Princeton Applied Research Bi-Stat potentiostat and a 616 Rotating Disk Electrode (RDE) setup. All tests were performed using 0.5 M H_2SO_4 electrolyte, an Ag/AgCl (sat. KCl) reference electrode, and a Pt wire counter electrode. The CVs swept from 1.2 to 0.0 to 1.2 V vs. Reversible Hydrogen Electrode (RHE).

Catalyst ink was prepared by adding 95 μL 5wt% Nafion in aliphatic alcohols and 350 μL 200 proof EtOH to 10 mg catalyst. This mixture was subsequently sonicated for an hour. Next, a 7 μL aliquot of catalyst ink was applied to the glassy carbon disk electrode and allowed to dry for 15 minutes. Before testing began the electrolyte was saturated with oxygen, then CVs were run at 50 mV/s until the polarization curves overlapped so that any gaseous species or impurities would be removed from the catalyst surface. Subsequently, CVs were run at 10 mV/s at 0, 100, and 1000 rpm in oxygen saturated electrolyte. Testing was repeated in argon sparged electrolyte to obtain a background.

The ORR activity, also called onset potential, was defined as the voltage at which the current from the 0 rpm oxygen scan was 10% greater than that of the argon background scan. Additional measures of performance are the peak potential, V_{pr}, which is defined as the voltage where the current minima occurred in the 0 rpm oxygen CV, and potential when -0.1 mA/cm^2 was reached, $V_{-0.1}$.

Statistical Design

The goal of using a statistical model was to be able to qualitatively compare the effects of various parameters on the activity of the Fe/N/C catalysts and to determine the efficacy of using a statistical model for analysis and predication of the catalytic activity of NPMC towards the ORR.

The first step in designing the model for the main section was to determine the response variables. The responses were chosen based on indicators that are found in the literature: onset potential, voltage when a given current was reached, and peak voltage during cyclic voltammetry (CV) with no rotation. These responses are described in the electrochemical testing section of the experimental methods.

The next step was to determine the factors for the model. The factors were chosen based on perceived influence on activity and what was discussed in the literature. They were: carbon black support, iron (acetate:nitrate) precursors, inert gas, reactive gas, and reactive gas pyrolysis duration.

The last steps were to determine the model order and number of runs. These are related because the order of a model and number of factors affect the required number of runs. To be practical, the model was kept at first order with no interaction terms. The number of runs (samples) was 16. Refer to Appendix A for more information concerning the experimental design and statistical analysis.

The model generated for statistical testing using JMP® was

$$y = \mu + CB_i + FeP_j + IG_k + PG_l + PD_m + \varepsilon$$

where μ = mean and $\boldsymbol{\varepsilon}$ = random error. Table 5 describes the factors and responses included in the model.

Table 5. Factors and Responses included in Main Section Statistical Model.

y (response)	CB_i	FeP_j	IG_k	PG_l	PD_m (min)
Onset potential	Ketjen Black (KB)	1:0	Argon	Ammonia	5
$V_{-0.1}$	Black Pearls (BP)	1:1	Nitrogen	Acetonitrile	20
V_{pr}		0:1			40

Note: CB denotes carbon black support, FeP denotes the ratio between iron precursors (acetate:nitrate) on an iron basis, IG denotes inert gas, PG denotes pyrolysis gas, and PD denotes pyrolysis duration.

The experimental results were analyzed using JMP® and the results will be discussed in the following section.

Results and Discussion

Main Section Results

The experimental results were analyzed using JMP® and the obtained results are presented based on factor.

Carbon Black Support

Ketjen black and Black pearls were used as supports for the samples in this study, and their effect on onset potential and $V_{-0.1}$ was not found to be statistically significant. The effect of carbon support on peak voltage was found to be significant with p-value of 0.0464. The parameter estimate for the effect of Ketjen black was -16.6 mV and 16.6 mV for Black pearls for the model

$$y = \mu + CB_i + PG_l + \varepsilon$$

The power obtained for the carbon support was 0.38 with an LSN of 22. Figure 9 compares the effect of Ketjen black to that of Black pearls. It is not surprising that the carbon support should be found to be statistically significant considering it has been noted to affect ORR activity.[67, 74] Moreover, Black pearls has more microporous surface area than Ketjen black, which enables greater active site formation.[69]

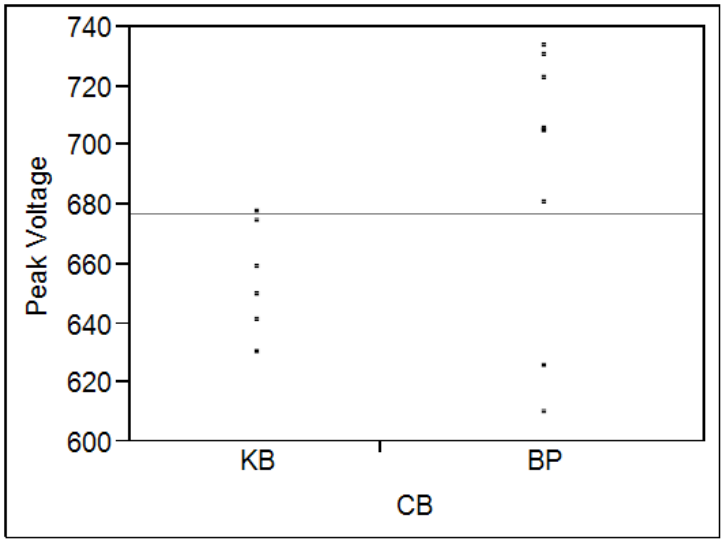

Figure 9. Comparison of Peak Voltage by Ketjen Black (KB) and Black Pearls (BP).

Iron Precursor Ratio

Iron(II) acetate and iron(III) nitrate•nonahydrate were used as precursors for the samples in this study. Their effect was not found to be statistically significant for all responses. The power of the iron precursor effect ranged from 0.0587 to 0.1505 and LSN from 67 to 674. These results are expected considering that many metal precursors have been used,[18, 24, 28] but found to not control the ORR activity.[70]

Inert Gas

Nitrogen and argon were used as the inert gases for the inert pyrolysis step in this study. Their effect was not found to be statistically significant for all responses. The power of the inert gas effect ranged from 0.0539 to 0.1158 and LSN from 99 to 1567. It

was expected that the effect of inert gas would not have a significant effect on the ORR activity.[79]

Pyrolysis Gas

Ammonia and acetonitrile were used as the reactive gases in the reactive gas pyrolysis step in this study. The effect of reactive gas on onset potential and $V_{-0.1}$ was not statistically significant. However, the effect of reactive gas on V_{pr} was found to be significant with p-value of 0.0177 for the model

$$y = \mu + CB_i + PG_l + \varepsilon$$

The parameter estimate for the effect of acetonitrile was -20.5 mV and 20.5 mV for ammonia. The power obtained for the reactive gas was 0.58 with LSN of 14. Figure 10 compares the effect of acetonitrile to that of ammonia.

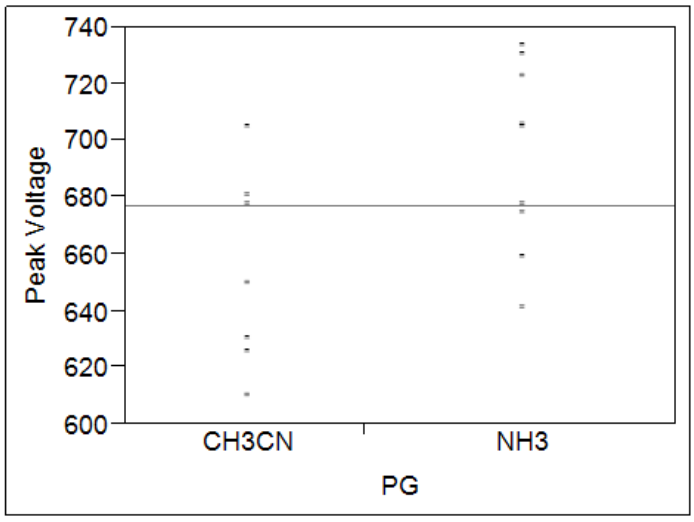

Figure 10. Comparison of V_{pr} (peak voltage) Obtained using either Ammonia or Acetonitrile as Pyrolysis Gas (PG).

These results are reasonable considering that the ORR activity has been found to correlate to the microporous surface area and ammonia is known to etch the carbon support, whereas acetonitrile causes deposition.

Pyrolysis Duration

The duration of the reactive pyrolysis was varied at 5, 20, and 40 minutes in this study. The effect of duration was not found to be statistically significant for all responses. The duration effect power ranged from 0.054 to 0.0736 with LSN from 255 to 1443. These results are expected considering that 5 to 12 minutes has been found to be sufficient for site formation.[76]

Overall Model

The effect size of the iron precursors, inert gas, and pyrolysis duration are likely the reason these factors were not found to be significant. Moreover, only V_{pr} a sensitive enough response for the experimental design to yield a statistically significant model

$$y = \mu + CB_i + PG_l + \varepsilon$$

where the parameter estimates are: acetonitrile: -20.5 mV, ammonia: 20.5 mV, Ketjen black: -16.6 mV, and Black pearls: 16.6 mV. The LSN for the carbon support factor was 22 and for the pyrolysis gas was 14. The overall model power was 0.22. The model Rsquare was 0.48, Rsquare Adjusted was 0.40, and Max Rsquare was 0.61. These results indicate that the model does not fit the data well, even though it is statistically significant.

The results obtained suggest that V_{pr} would be more viable as a response for future analysis than onset potential and $V_{-0.1}$. Perhaps this is attributable to its theoretical background.[80] However, the experimental design was fairly simple in that it did not include interactions between factors, and this could have affected the perceived sensitivity of the other factors and contributed to the poor fit of the obtained model.

Acid Wash Results

Figure 11 displays the CVs of the acid washed samples and Figure 12 presents a close up. Two trends are apparent: first is that acid washed samples show reduced activity compared to unwashed samples and the second is that an ammonia treatment increases activity.

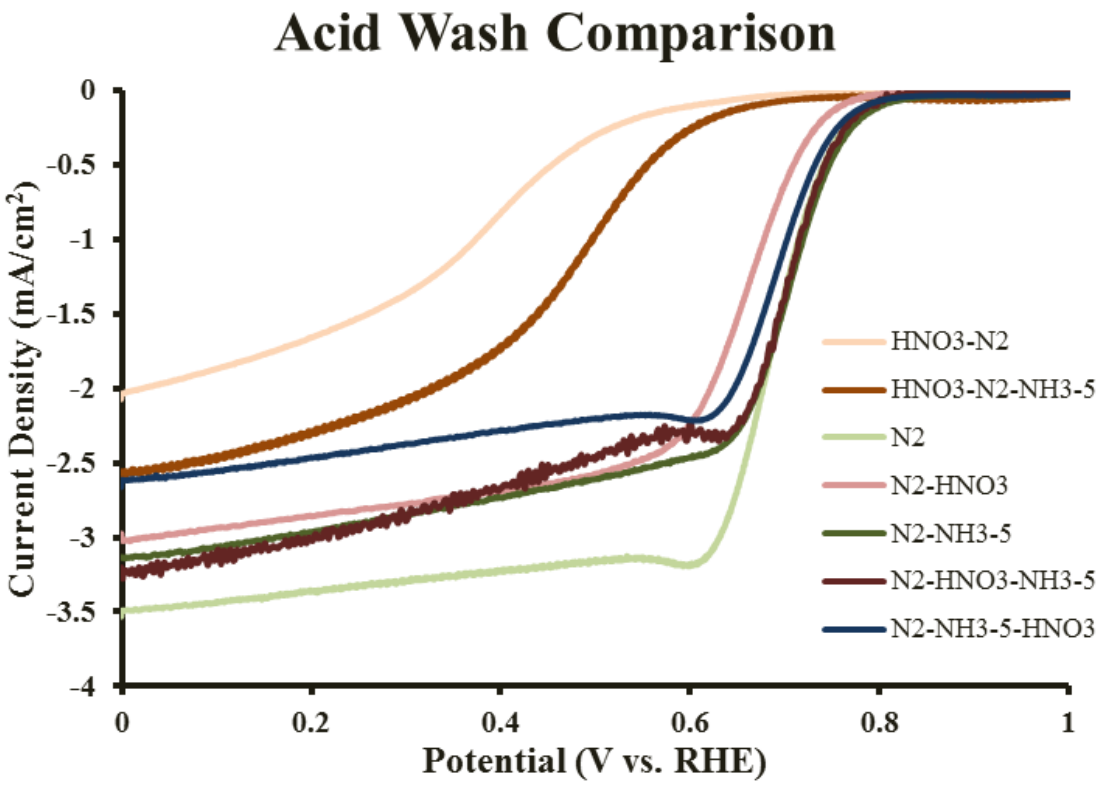

Figure 11. Comparison of Activity of Acid Washed Samples.

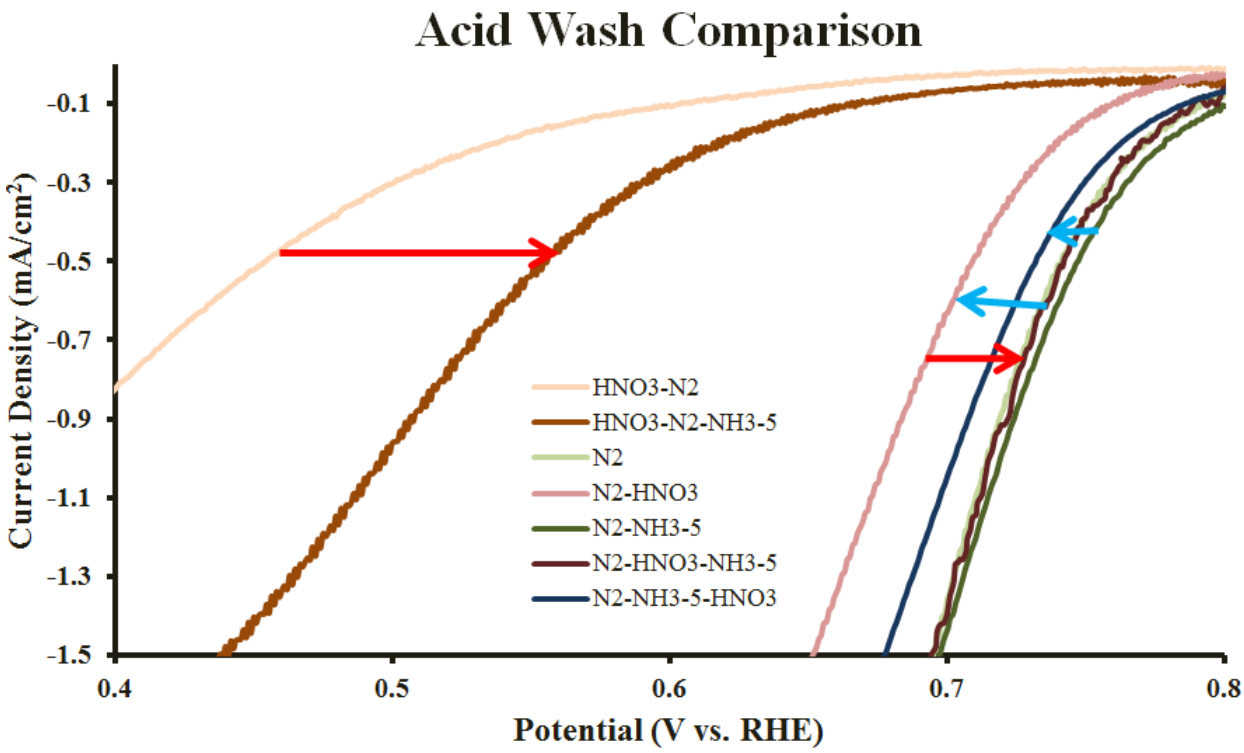

Figure 12. Close-up of Acid Wash Comparison with Red Arrows Showing Ammonia Activation and Blue Arrows Acid Wash Deactivation.

Note that the legend indicates the order of treatments.

The decrease in activity after acid washing could be attributed to leaching of iron from the carbon support.[71] Table 6 describes the preparation and activity of the acid washed samples.

Table 6. Description of Acid Washed Samples and their Activity.

Sample	Carbon Support	Acetate: Nitrate Precursors	Inert Gas	Reactive Gas	Reactive Pyrolysis Duration (min)	Onset Potential (mV)	$V_{-0.1}$ (mV)	Acid Wash (1M HNO3)
1	KB	1:0	N_2	N/A	N/A	630	602	Before inert pyrolysis
2	KB	1:0	N_2	NH_3	5	649	657	Before inert pyrolysis
3	KB	1:0	N_2	N/A	N/A	815	796	N/A
4	KB	1:0	N_2	N/A	N/A	763	809	After inert pyrolysis
5	KB	1:0	N_2	NH_3	5	852	806	N/A
6	KB	1:0	N_2	NH_3	5	790	799	Between inert and reactive pyrolyses
7	KB	1:0	N_2	NH_3	5	806	784	After reactive pyrolysis

Third Heat Treatment Results

Figure 13 displays the CVs of the thrice heat treated samples. The difference in activity between the N_2-NH_3-CH_3CN and N_2-CH_3CN-NH_3 samples could be attributed to carbon deposition over active sites formed by ammonia etching and/or other surface modifications caused by heat treatment in acetonitrile.

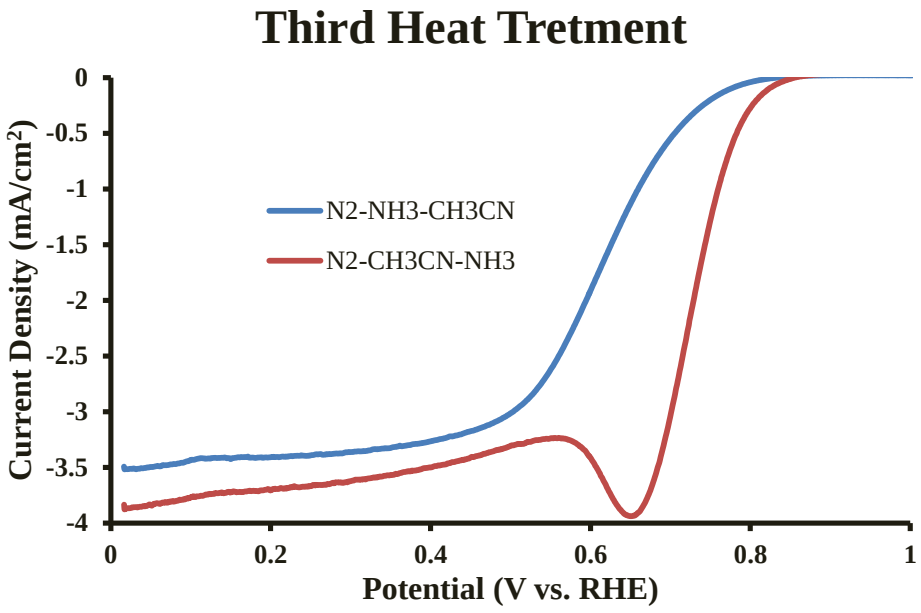

Figure 13. Comparison of Activity of Third Heat Treatment Samples.

Note that the legend indicates the order of gases used.

Table 9 describes the preparation and activity of the third heat treatment samples.

Table 7. Description of Third Heat Treatment Samples and their Activity.

Sample	Carbon Support	Acetate: Nitrate Precursors	Inert Gas	First Reactive Gas	First Reactive Pyrolysis Duration (min)	Second Reactive Gas	Second Reactive Pyrolysis Duration (min)	Onset Potential (mV)	$V_{-0.1}$ (mV)
1	BP	1:0	N_2	NH_3	20	CH_3CN	20	807	769
2	BP	1:0	N_2	CH_3CN	20	NH_3	20	822	822

Conclusions

Although most of the statistical results obtained were not significant, there is still much that can be learned from them. For instance, the Fe/N/C catalyst preparation procedure is a fairly robust process with respect to activity. The means and corresponding standard deviations for the responses were 677 mV & 39 mV, 815 mV & 20 mV, and 842 mV & 10mV for V_{pr}, $V_{-0.1}$, and onset potential respectively. On another note, the LSN values obtained indicate that using onset potential or $V_{-0.1}$ as an indicator of activity requires more samples (at least for the models used), and that V_{pr} is a more practical indicator of activity for statistical analysis. The results also demonstrate that modeling of NPMC activity towards the ORR is feasible. However, the responses and experimental design should be chosen carefully. The design should also include the ability to estimate interaction terms between factors, as ignoring them could contribute to poor fit to the data. Finally, the procedure used in the main section appears to either be close to an optimum[81] and/or the factors that were not varied (i.e. ballmilling duration, gas flow rates, etc.) are more influential on activity.

Acid washing appeared to deactivate the Fe/N/C catalysts, which could be attributed to iron removal. Further stability testing should be conducted to see if the activity loss comes with an increase in stability and if that stability increase would be valuable for other more active Fe/N/C catalysts.

The third heat treatment seemed to deactivate the Fe/N/C catalysts somewhat, seeing as their onset potentials were between two and three standard deviations below the mean of the main section samples. Perhaps different carbon morphologies were produced with greater interfacial resistance than those produced with the N_2-CH_3CN-NH_3 sample. The difference in activity between the third heat treatment samples might be due to deposition over active sites formed by the ammonia etching and/or surface modifications caused by the heat treatments.

Appendix A

Experimental Design

The experimental design chosen for this thesis was D-optimal. This was selected because D-optimal designs provide more precise estimates of model parameters.[82] This design was modified based on the inability to use four of the catalysts. The original design is presented in Table 8 and the modified design is presented in Table 9.

Table 8. Original D-Optimal Experimental Design.

Sample	Carbon Support	Acetate: Nitrate Precursors	Inert Gas	Reactive Gas	Reactive Gas Pyrolysis Duration (min)
1	KB	1:0	N_2	CH_3CN	5
2	BP	1:0	Ar	CH_3CN	40
3	KB	1:1	N_2	NH_3	40
4	KB	1:1	Ar	NH_3	5
5	BP	1:0	Ar	NH_3	5
6	BP	1:0	N_2	NH_3	40
7	BP	0:1	Ar	CH_3CN	5
8	KB	1:0	N_2	CH_3CN	20
9	BP	1:0	N_2	NH_3	5
10	BP	1:1	Ar	CH_3CN	20
11	KB	0:1	N_2	NH_3	5
12	KB	0:1	N_2	CH_3CN	40
13	BP	1:1	N_2	NH_3	20
14	BP	1:1	N_2	CH_3CN	5
15	BP	0:1	Ar	NH_3	40
16	KB	1:0	Ar	CH_3CN	5
17	KB	0:1	Ar	NH_3	20
18	KB	1:0	Ar	NH_3	20
19	BP	0:1	N_2	CH_3CN	20
20	KB	1:1	Ar	CH_3CN	40

Table 9. Modified Experimental Design.

Sample	Carbon Support	Acetate: Nitrate Precursors	Inert Gas	Reactive Gas	Reactive Pyrolysis Duration (min)
1	BP	1:0	Ar	CH_3CN	40
2	KB	1:1	N_2	NH_3	40
3	KB	1:1	Ar	NH_3	5
4	BP	1:0	Ar	NH_3	5
5	BP	1:0	N_2	NH_3	40
6	BP	0:1	Ar	CH_3CN	5
7	KB	1:0	N_2	CH_3CN	20
8	BP	1:0	N_2	NH_3	5
9	BP	1:1	Ar	CH_3CN	20
10	KB	0:1	N_2	NH_3	5
11	BP	1:1	N_2	NH_3	20
12	BP	0:1	Ar	NH_3	40
13	KB	1:0	Ar	CH_3CN	5
14	KB	1:0	Ar	NH_3	20
15	BP	0:1	N_2	CH_3CN	20
16	KB	1:1	Ar	CH_3CN	40

Model and Power Analysis

The first model generated was tested for each response – onset potential, peak voltage, and current density – and it was

$$y = \mu + CB_i + FeP_j + IG_k + PG_l + PD_m + \varepsilon$$

where μ = mean and $\boldsymbol{\varepsilon}$ = random error. Table 10 describes the factors and responses included in the model.

Table 10. Factors and Responses included in Main Section Statistical Model.

y (response)	CB_i	FeP_j	IG_k	PG_l	PD_m (min)
Onset potential	Ketjen Black (KB)	1:0	Argon	Ammonia	5
$V_{-0.1}$	Black Pearls (BP)	1:1	Nitrogen	Acetonitrile	20
V_{pr}		0:1			40

The statistical analysis proceeded by first checking the significance of the model. If the model was not significant, then the significance of the parameter estimates was analyzed and a factor was removed from the model based on how close the p-value was to one. The model was then retested. This procedure was used for all of the responses using various combinations of the factors. The lists of the combinations used are presented in Tables 11 – 13.

Table 11. List of Models Tested and Corresponding p-values for the Response of Onset Potential.

Model Factors	p-value (Prob>F)	Rsquare	Max Rsquare
CB, FeP, IG, PG, PD	0.9878	0.1206	
CB, FeP, PG, PD	0.9693	0.1162	0.9620
CB, FeP, PG	0.8818	0.0938	0.4306
CB, FeP, PD	0.9857	0.0551	0.6698
CB, PG, PD	0.9393	0.0642	0.6729
CB, FeP, IG, PG	0.9518	0.0939	0.8614
CB, FeP	0.8973	0.0466	0.0870
CB	0.7735	0.0061	
FeP, PG, PD	0.9438		
FeP, PG, PD, FeP*PG	0.9714		
FeP, PG, PD, FeP*PD	0.3800		
FeP, PD	0.9725		
FeP, PD, FeP*PD	0.4953		
FeP, PG, PD, PG*PD	0.9881		
PG, PD	0.8623		
PG, PD, PG*PD	0.9722		
FeP	0.7925	0.0351	
CB, FeP, PG, PD, FeP*PD	0.2538		
CB, FeP, IG, PG, PD, FeP*PD	0.0533		
PG	0.4297	0.0451	
PD	0.9674	0.0050	

Table 12. List of Models Tested and Corresponding p-values for the Response of $V_{-0.1}$ (Current Density).

Model Factors	p-value (Prob>F)	Rsquare	Max Rsquare
CB, FeP, IG, PG, PD	0.9395	0.2028	
CB, FeP, IG, PG	0.8201	0.1759	0.8534
FeP, IG, PG	0.6994	0.1680	0.7565
FeP, PG	0.5380	0.1995	
FeP	0.4914	0.1596	0.2748
CB	0.6905	0.0116	
CB, FeP	0.6887		
CB, FeP, CB*FeP	0.8752		
CB, FeP, PG	0.7009		
CB, FeP, PG, PG*CB	0.1998		
CB, FeP, PG, PG*FeP	0.7462		
CB, FeP, PD	0.8814		
CB, FeP, PD, CB*PD	0.7689		
CB, FeP, PD, PG	0.8984		
CB, FeP, PD, PG, PD*PG	0.9698		
CB, FeP, PD, PG, CB*PG	0.4216		
CB, FeP, PD, PG, CB*PG, FeP*PG	0.6246		
CB, PG, CB*PG	0.3803		
IG	0.5704	0.0235	
IG, CB	0.7893		
IG, CB, PG	0.8052		
IG, CB, PG, FeP	0.8201		
IG, CB, PG, FeP, CB*PG	0.3271		
IG, CB, PG, CB*PG	0.5586		

Table 13. List of Models Tested and Corresponding p-values for the Response of Vpr (Peak Voltage).

Model Factors	p-value (Prob>F)	Rsquare	Max Rsquare
CB, FeP, IG, PG, PD	0.3780	0.5221	
CB, FeP, IG, PG	0.1633	0.5006	0.9935
CB, IG, PG	0.0413*	0.4840	0.8035
CB, FeP, PG	0.0853		
CB, FeP, PG, PG*CB	0.0249*		
CB, PG	0.0141*	0.4806	0.6056
CB, PG, CB*PG	0.0090*		
CB, PG, CB*PG, PD	0.0559		
CB, FeP, PG, CB*PG, FeP*PG	0.1133		

Note that an asterisk indicates a significant model

After obtaining models that were significant, the power of the factors was determined. One limitation of the JMP® software is that it is unable to perform power analysis of categorical interaction terms (*e.g.* PG*CB); thus, the power of models that

contain interaction terms could not be fully determined. As a result, only the power analysis of the model

$$y = \mu + CB_i + PG_l + \varepsilon$$

where y is the peak voltage, will be reported. Prior to power analysis, it was confirmed that the studentized residuals were normally distributed. This analysis is presented below.

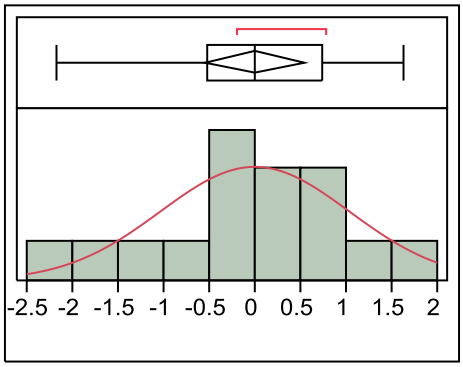

Figure 14. Normal Distribution of Studentized Residuals of Model for Peak Voltage.

Note: The mean and standard deviation are listed below.

Table 14. Quantiles of Studentized Residuals of Model for Peak Voltage.

100.0%	maximum	1.62231
99.5%		1.62231
97.5%		1.62231
90.0%		1.43641
75.0%	quartile	0.73118
50.0%	median	0.00944
25.0%	quartile	-0.5315
10.0%		-1.7578
2.5%		-2.1741
0.5%		-2.1741
0.0%	minimum	-2.1741

Table 15. Moments of Studentized Residuals of Model for Peak Voltage.

Mean	0.0007485
Std Dev	1.0364542
Std Err Mean	0.2591136
Upper 95% Mean	0.5530359
Lower 95% Mean	-0.551539
N	16

Table 16. Fitted Normal Parameter Estimates of Studentized Residuals of Model for Peak Voltage.

Type	Parameter	Estimate	Lower 95%	Upper 95%
Location	μ	0.0007485	-0.551539	0.5530359
Dispersion	σ	1.0364542	0.7656338	1.6041111

Table 17. Goodness-of-Fit Test (Shapiro-Wilk W Test)
for Studentized Residuals of Model for Peak Voltage.

W		Prob<W
0.959921		0.6603

Note: Ho = The data is from the Normal distribution. Small p-values reject Ho.

Since the studentized residuals were normally distributed, the power analysis could be performed without needing to exclude any points. The results of this analysis are presented below.

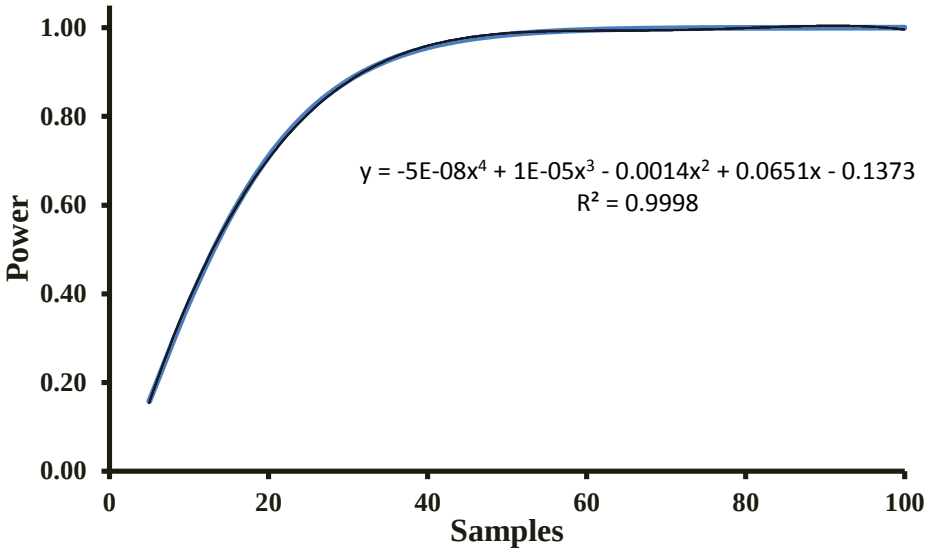

Figure 15. Power of Pyrolysis Gas Factor in the Model for Peak Voltage.

The power of the pyrolysis gas factor was estimated assuming $\alpha = 0.05$, the standard error of the residual error (σ) = 33.74, and the raw effect size (δ) = 20 mV. Using these assumptions, an LSN of 14 was obtained. When combined with a well-fitting polynomial trendline, a power of 0.58 was obtained.

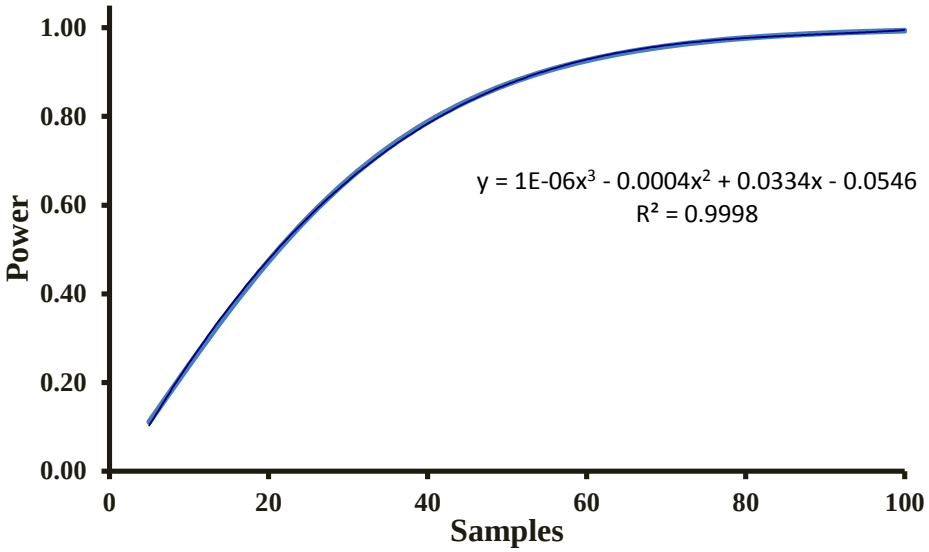

Figure 16. Power of Carbon Support Factor in the Model for Peak Voltage.

The power of the carbon support factor was estimated assuming $\alpha = 0.05$, the standard error of the residual error (σ) = 36.05, and the raw effect size (δ) = 16 mV. Using these assumptions, an LSN of 22 was obtained. When combined with a well-fitting polynomial trendline, a power of 0.38 was obtained.

The power of a multifactor model is equal to the product of the powers of the individual factors; thus, the model power equals

$$1 - \beta = 0.58*0.38 = 0.22$$

The predictive qualities of this model are presented below.

Table 18. Summary of Fit for Peak Voltage Model.

RSquare	0.480697
RSquare Adj	0.400804
Root Mean Square Error	29.88647
Mean of Response	677
Observations (or Sum Wgts)	16

Table 19. Analysis of Variance for Peak Voltage Model.

Source	DF	Sum of Squares	Mean Square	F Ratio
Model	2	10748.383	5374.19	6.0168
Error	13	11611.617	893.20	**Prob > F**
C. Total	15	22360.000		0.0141*

Table 20. Lack of Fit Results of Peak Voltage Model.

Source	DF	Sum of Squares	Mean Square	F Ratio
Lack Of Fit	1	2792.400	2792.40	3.7995
Pure Error	12	8819.217	734.93	**Prob > F**
Total Error	13	11611.617		0.0750
				Max RSq
				0.6056

Table 21. Parameter Estimates for Peak Voltage Model.

Term		Estimate	Std Error	t Ratio	Prob>|t|
Intercept		672.37097	7.591172	88.57	<.0001*
CB[KB]		-16.57863	7.531632	-2.20	0.0464*
PG[CH3CN]		-20.45363	7.531632	-2.72	0.0177*

As the “Lack of Fit” analysis and Rsquare value demonstrate, the model does not fit the data well even though it is significant. This could be related to the low power obtained for the model, the small number of factors used, or the actual effect size of the peak voltage.

References

1. Fuel Cell Basics. http://americanhistory.si.edu/fuelcells/basics.htm (accessed 08-06-2012).

2. Comparison of Fuel Cell Technologies. http://www1.eere.energy.gov/hydrogenandfuelcells/fuelcells/pdfs/fc_comparison_chart.pdf (accessed 05-2012).

3. Rand, D. A. J.; Dell, R. M., *Hydrogen energy : challenges and prospects*. Royal Society of Chemistry: Cambridge, UK, 2008.

4. Fuel cell operation. http://www.esru.strath.ac.uk/EandE/Web_sites/00-01/fuel_cells/fuel%20cell%20operation.html (accessed 06-28-2012).

5. Brian D James; Jeff Kalinoski; Baum, K. Manufacturing Cost Analysis Of Fuel Cell Systems. http://www.hydrogen.energy.gov/pdfs/review11/fc018_james_2011_o.pdf (accessed 07-02-2012).

6. KITCO Platinum. http://www.kitco.com/charts/liveplatinum.html (accessed 05-2012).

7. TIAX *Platinum Availability and Economics for PEMFC Commercialization*; U.S. DOE Energy Efficiency & Renewable Energy: 2003.

8. Dunleavy, J. K., Sulfur as a Catalyst Poison. *Platinum Metals Review* 2006, 50.

9. FCHEA Hydrogen Production Overview. http://www.fchea.org/core/import/PDFs/factsheets/Hydrogen%20Production%20Overview_NEW.pdf (accessed 08-24-2012).

10. NREL Hydrogen Production and Delivery. http://www.nrel.gov/hydrogen/proj_production_delivery.html (accessed 08-24-2012).

11. von Deak, D.; Singh, D.; King, J. C.; Ozkan, U. S., Use of carbon monoxide and cyanide to probe the active sites on nitrogen-doped carbon catalysts for oxygen reduction. *Applied Catalysis B, Environmental* 2012, 113-114, 126-133.

12. James, B. D., Kalinoski, J. A, Baum, K. N. *Mass Production Cost Estimation for Direct H2 PEM Fuel Cell Systems for Automotive Applications: 2010 Update*; Directed Technologies Inc.: 2010.

13. Frassinelli, M. The Hindenburg 75 years later: Memories time cannot erase. http://www.nj.com/news/index.ssf/2012/05/the_hindenberg_75_years_later.html (accessed 06-11-2013).

14. Grossman, D. The Hindenburg Disaster. http://www.airships.net/hindenburg/disaster (accessed 06-11-2013).

15. Gasteiger, H. A.; Kocha, S. S.; Sompalli, B.; Wagner, F. T., Activity benchmarks and requirements for Pt, Pt-alloy, and non-Pt oxygen reduction catalysts for PEMFCs. *Applied Catalysis B: Environmental* 2005, 56, 9-35.

16. Wagner, F. T., Gasteiger, Hubert A., Yan, Susan In *What performance would non-Pt cathode catalysts need to achieve to be practical for transportation? or The Importance of A/cm3*, DOE Workshop on Non-Platinum Electrocatalysts, New Orleans, LA, New Orleans, LA, 2003.

17. Jasinski, R., A new fuel cell cathode catalyst. *Nature* 1964, 201, 1212.

18. Matter, P. H.; Biddinger, E. J.; Ozkan, U. S., Non-precious metal oxygen reduction catalysts for PEM fuel cells. In *Catalysis*, Spivey, J. J., Ed. The Royal Society of Chemistry: Cambridge, UK, 2007; Vol. 20, pp 338-361.

19. Jasinski, R., Cobalt phthalocyanine as a fuel cell cathode. *Journal of the Electrochemical Society* 1965, 112, 526-528.

20. Yeager, E., Electrocatalysts for O_2 reduction. *Electrochimica Acta* 1984, 29, 1527-1537.

21. Yeager, E., Dioxygen electrocatalysis: Mechanisms in relation to catalyst structure. *Journal of Molecular Catalysis* 1986, 38, 5-25.

22. Barazzouk, S.; Lefevre, M.; Dodelet, J.-P., Oxygen reduction in PEM fuel cells: Fe-based electrocatalysts made with high surface area activated carbon supports. *Journal of the Electrochemical Society* 2009, 156, B1466-B1474.

23. Biddinger, E. J. Nitrogen-containing carbon nanofibers as non-noble metal cathode catalysts in PEM and direct methanol fuel cells. http://rave.ohiolink.edu/etdc/view.cgi?acc%5Fnum=osu1274389015.

24. Jahnke, H.; Schonborn, M.; Zimmerman, G., Organic dyestuffs as catalysts for fuel cells. *Fortschr. Chem. Forsch.* 1976, 61, 133.

25. van Veen, J. A. R.; van Baar, J. F.; Kroese, K. J., Effect of heat treatment on the performance of carbon-supported transition-metal chelates in the electrochemical reduction of oxygen. *Chem. Soc., Faraday Trans. I* 1981, 77, 2827.

26. Wiesener, K., N_4-chelates as electrocatalysts for cathodic oxygen reduction. *Electrochimica Acta* 1986, 31, 1073-1078.

27. Gupta, S.; Tryk, D.; Bae, I.; Aldred, W.; Yeager, E., Heat-treated polyacrylonitrile-based catalysts for oxygen electroreduction. *Journal of Applied Electrochemistry* 1989, 19, 19.

28. Bezerra, C. W. B.; Zhang, L.; Lee, K.; Liu, H.; Marques, A. L. B.; Marques, E. P.; Wang, H.; Zhang, J., A review of Fe-N/C and Co-N/C catalysts for the oxygen reduction reaction. *Electrochimica Acta* 2008, 53, 4937-4951.

29. Gewirth, A. A.; Thorum, M. S., Electroreduction of dioxygen for fuel-cell applications: Materials and challenges. *Inorganic Chemistry* 2010, 49, 3557-3566.

30. Shao, Y.; Sui, J.; Yin, G.; Gao, Y., Nitrogen-doped carbon nanostructures and their composites as catalytic materials for proton exchange membrane fuel cell. *Applied Catalysis B: Environmental* 2008, 79, 89-99.

31. Wang, B., Recent development of non-platinum catalysts for oxygen reduction reaction. *Journal of Power Sources* 2005, 152, 1-15.

32. Gruenig, G.; Wiesener, K.; Gamburzev, S.; Iliev, I.; Kaisheva, A., Investigations of catalysts from the pyrolyzates of cobalt-containing and metal-free dibenzotetraazaannulenes on active carbon for oxygen electrodes in an acid medium. *Journal of Electroanalytical Chemistry and Interfacial Electrochemistry* 1983, 159, 155-162.

33. Matter, P. H.; Wang, E.; Ozkan, U. S., Preparation of nanostructured nitrogen-containing carbon catalysts for the oxygen reduction reaction from SiO_2 and MgO supported metal particles. *Journal of Catalysis* 2006, 243, 395-403.

34. Charreteur, F.; Jaouen, F.; Ruggeri, S.; Dodelet, J.-P., Fe/N/C non-precious catalysts for PEM fuel cells: Influence of the structural parameters of pristine commercial carbon blacks on their activity for oxygen reduction. *Electrochimica Acta* 2008, 53, 2925-2938.

35. Endo, M., Grow carbon fibers in the vapor phase. *Chemtech* 1988, 18, 568-576.

36. Baker, R. T. K.; Alonzo, J. R.; Dumesic, J. A.; Yates, D. J. C., Effect of the surface state of iron on filamentous carbon formation. *Journal of Catalysis* 1982, 77, 74-84.

37. Oberlin, A.; Endo, M.; Koyama, T., Filamentous growth of carbon through benzene decomposition. *J. Cryst. Growth* 1976, 32, 335-349.

38. Boehm, H. P., Carbon from carbon monoxide disproportionation on nickel and iron catalysts: Morphological studies and possible growth mechanisms. *Carbon* 1973, 11, 583-590.

39. Baker, R., Formation of filamentous carbon from iron, cobalt and chromium catalyzed decomposition of acetylene. *Journal of Catalysis Journal of Catalysis* 1973, 30, 86-95.

40. Baker, R. T. K.; Barber, M. A.; Harris, P. S.; Feates, F. S.; Waite, R. J., Nucleation and growth of carbon deposits from the nickel catalyzed decomposition of acetylene. *Journal of Catalysis* 1972, 26, 51-62.

41. Ning, G.; Wei, F.; Wen, Q.; Luo, G.; Wang, Y.; Jin, Y., Improvement of Fe/MgO Catalysts by Calcination for the Growth of Single- and Double-Walled Carbon Nanotubes. *The Journal of Physical Chemistry B* 2005, 110, 1201-1205.

42. Coquay, P.; Peigney, A.; De Grave, E.; Vandenberghe, R. E.; Laurent, C., Carbon Nanotubes by a CVD Method. Part II: Formation of Nanotubes from (Mg, Fe)O Catalysts. *The Journal of Physical Chemistry B* 2002, 106, 13199-13210.

43. Ramesh, P.; Okazaki, T.; Taniguchi, R.; Kimura, J.; Sugai, T.; Sato, K.; Ozeki, Y.; Shinohara, H., Selective Chemical Vapor Deposition Synthesis of Double-Wall Carbon Nanotubes on Mesoporous Silica. *The Journal of Physical Chemistry B* 2004, 109, 1141-1147.

44. Hata, K., Water-Assisted Highly Efficient Synthesis of Impurity-Free Single-Walled Carbon Nanotubes. *Science Science* 2004, 306, 1362-1364.

45. Hafner, J. H.; Bronikowski, M. J.; Azamian, B. R.; Nikolaev, P.; Rinzler, A. G.; Colbert, D. T.; Smith, K. A.; Smalley, R. E., Catalytic growth of single-wall carbon nanotubes from metal particles. *Chemical Physics Letters* 1998, 296, 195-202.

46. Cassell, A. M. R. J. A. K. J. D. H., Large scale CVD synthesis of single-walled carbon nanotubes.(chemical vapor deposition). *Journal of Physical Chemistry B* 1999, 103.

47. Ago, H.; Nakamura, K.; Uehara, N.; Tsuji, M., Roles of Metal−Support Interaction in Growth of Single- and Double-Walled Carbon Nanotubes Studied with Diameter-Controlled Iron Particles Supported on MgO. *The Journal of Physical Chemistry B* 2004, 108, 18908-18915.

48. Ning, G.; Liu, Y.; Wei, F.; Wen, Q.; Luo, G., Porous and Lamella-like Fe/MgO Catalysts Prepared under Hydrothermal Conditions for High-Yield Synthesis of Double-Walled Carbon Nanotubes. *The Journal of Physical Chemistry C* 2007, 111, 1969-1975.

49. Ago, H.; Nakamura, K.; Imamura, S.; Tsuji, M., Growth of double-wall carbon nanotubes with diameter-controlled iron oxide nanoparticles supported on MgO. *Chemical Physics Letters* 2004, 391, 308-313.

50. Colomer, J. F.; Stephan, C.; Lefrant, S.; Van Tendeloo, G.; Willems, I.; Kónya, Z.; Fonseca, A.; Laurent, C.; Nagy, J. B., Large-scale synthesis of single-wall carbon nanotubes by catalytic chemical vapor deposition (CCVD) method. *Chemical Physics Letters* 2000, 317, 83-89.

51. Tang, S.; Zhong, Z.; Xiong, Z.; Sun, L.; Liu, L.; Lin, J.; Shen, Z. X.; Tan, K. L., Controlled growth of single-walled carbon nanotubes by catalytic decomposition of CH4 over Mo/Co/MgO catalysts. *Chemical Physics Letters* 2001, 350, 19-26.

52. Flahaut, E.; Govindaraj, A.; Peigney, A.; Laurent, C.; Rousset, A.; Rao, C. N. R., Synthesis of single-walled carbon nanotubes using binary (Fe, Co, Ni) alloy nanoparticles prepared in situ by the reduction of oxide solid solutions. *Chemical Physics Letters* 1999, 300, 236-242.

53. Qingwen, L.; Hao, Y.; Yan, C.; Jin, Z.; Zhongfan, L., A scalable CVD synthesis of high-purity single-walled carbon nanotubes with porous MgO as support material. *Journal of Materials Chemistry* 2002, 12, 1179-1183.

54. Flahaut, E.; Bacsa, R.; Peigney, A.; Laurent, C., Gram-scale CCVD synthesis of double-walled carbon nanotubes. *Chemical Communications* 2003, 0, 1442-1443.

55. Lyu, S. C.; Liu, B. C.; Lee, S. H.; Park, C. Y.; Kang, H. K.; Yang, C. W.; Lee, C. J., Large-Scale Synthesis of High-Quality Single-Walled Carbon Nanotubes by Catalytic Decomposition of Ethylene. *The Journal of Physical Chemistry B* 2004, 108, 1613-1616.

56. Lyu, S. C.; Liu, B. C.; Lee, S. H.; Park, C. Y.; Kang, H. K.; Yang, C.-W.; Lee, C. J., Large-Scale Synthesis of High-Quality Double-Walled Carbon Nanotubes by Catalytic Decomposition of n-Hexane. *The Journal of Physical Chemistry B* 2004, 108, 2192-2194.

57. Matter, P. H.; Wang, E.; Millet, J.-M. M.; Ozkan, U. S., Characterization of the iron phase in CN_x-based oxygen reduction reaction catalysts. *Journal of Physical Chemistry C* 2007, 111, 1444-1450.

58. Lefevre, M.; Dodelet, J. P.; Bertrand, P., O_2 reduction in PEM fuel cells: Activity and active site structural information for catalysts obtained by the pyrolysis at high temperatures of Fe precursors. *Journal of Physical Chemistry B* 2000, 104, 11238.

59. Faubert, G., Côté, R., Dodelet, J.P., Lefèvre, M., Bertrand, P., Oxygen reduction catalysts for polymer electrolyte fuel cells from the pyrolysis of Fe^{II} acetate adsorbed on 3,4,9,10-perylenetetracarboxylic dianhydride. *Electrochimica Acta* 1999, 44, 2589.

60. He, P.; Lefebvre, M.; Faubert, G.; Dodelet, J. P., Oxygen reduction catalysts for polymer electrolyte fuel cells from the pyrolysis of various transition metal acetates adsorbed on 3,4,9,10-perylenetetracarboxylic dianhydride. *Journal of New Materials for Electrochemical Systems* 1999, 2, 243-251.

61. Lalande, G.; Cote, R.; Guay, D.; Dodelet, J. P.; Weng, L. T.; Bertrand, P., Is nitrogen important in the formation of Fe-based catalysts for oxygen reduction in solid polymer fuel cells? *Electrochimica Acta* 1997, 42, 1379.

62. Dignard-Bailey, L.; Trudeau, M. L.; Joly, A.; Schulz, R.; Lalande, G.; Guay, D.; Dodelet, J. P., Graphitization and particle size analysis of pyrolyzed cobalt phthalocyanine/carbon catalysts for oxygen reduction in fuel cells. *Journal of Materials Research* 1994, 9, 3203-3209.

63. Matter, P. H.; Zhang, L.; Ozkan, U. S., The role of nanostructure in nitrogen-containing carbon catalysts for the oxygen reduction reaction. *Journal of Catalysis* 2006, 239, 83-96.

64. Matter, P. H.; Wang, E.; Arias, M.; Biddinger, E. J.; Ozkan, U. S., Oxygen reduction reaction catalysts prepared from acetonitrile pyrolysis over alumina supported metal particles. *Journal of Physical Chemistry B* 2006, 110, 18374-18384.

65. Matter, P. H.; Ozkan, U. S., Non-metal catalysts for dioxygen reduction in an acidic electrolyte. *Catalysis Letters* 2006, 109, 115-123.

66. Medard, C.; Lefevre, M.; Dodelet, J. P.; Jaouen, F.; Lindbergh, G., Oxygen reduction by Fe-based catalysts in PEM fuel cell conditions: Activity and selectivity of the catalysts obtained with two Fe precursors and various carbon supports. *Electrochimica Acta* 2006, 51, 3202-3213.

67. Jaouen, F.; Charreteur, F.; Dodelet, J. P., Fe-based catalysts for oxygen reduction in PEMFCs: Importance of the disordered phase of the carbon support. *Journal of the Electrochemical Society* 2006, 153, A689-A698.

68. Tian, J.; Birry, L.; Jaouen, F.; Dodelet, J. P., Fe-based catalysts for oxygen reduction in proton exchange membrane fuel cells with cyanamide as nitrogen precursor and/or pore-filler. *Electrochimica Acta* 2011, 56, 3276-3285.

69. Jaouen, F.; Proietti, E.; Lefevre, M.; Chenitz, R.; Dodelet, J. P.; Chung, H. T.; Johnston, C. M.; Zelenay, P., Recent advances in non-precious metal catalysis for oxygen-reduction reaction in polymer electrolyte fuel cells. *Energy and Environmental Science* 2011, 4, 114-130.

70. Jaouen, F.; Herranz, J.; Lefevre, M.; Dodelet, J.-P.; Kramm, U. I.; Herrmann, I.; Bogdanoff, P.; Maruyama, J.; Nagaoka, T.; Garsuch, A.; Dahn, J. R.; Olson, T. S.; Pylypenko, S.; Atanassov, P.; Ustinov, E. A., Cross-laboratory experimental study of non-noble-metal electrocatalysts for the oxygen reduction reaction. *ACS Applied Materials & Interfaces* 2009, 1, 1623-1639.

71. Proietti, E.; Ruggeri, S.; Dodelet, J.-P., Fe-based electrocatalysts for oxygen reduction in PEMFCs using ballmilled graphite powder as a carbon support. *Journal of the Electrochemical Society* 2008, 155, B340-B348.

72. Proietti, E.; Dodelet, J. P., Ballmilling of carbon supports to enhance the performance of Fe-based electrocatalysts for oxygen reduction in PEM fuel cells. *ECS Transactions* 2008.

73. Lefevre, M.; Dodelet, J.-P., Fe-based electrocatalysts made with microporous pristine carbon black supports for the reduction of oxygen in PEM fuel cells. *Electrochimica Acta* 2008, 53, 8269-8276.

74. Ruggeri, S.; Dodelet, J.-P., Influence of structural properties of pristine carbon blacks on activity of Fe/N/C cathode catalysts for PEFCs. *Journal of the Electrochemical Society* 2007, 154, B761-B769.

75. Herranz, J.; Lefevre, M.; Larouche, N.; Stansfield, B.; Dodelet, J.-P., Step-by-step synthesis of non-noble metal electrocatalysts for O_2 reduction under proton exchange membrane fuel cell conditions. *Journal of Physical Chemistry C* 2007, 111, 19033-19042.

76. Jaouen, F.; Lefevre, M.; Dodelet, J.-P.; Cai, M., Heat-treated Fe/N/C catalysts for O_2 electroreduction: Are active sites hosted in micropores? *Journal of Physical Chemistry B* 2006, 110, 5553-5558.

77. Bron, M.; Fiechter, S.; Hilgendorff, M.; Bogdanoff, P., Catalysts for oxygen reduction from heat-treated carbon-supported iron phenantroline complexes. *Journal of Applied Electrochemistry* 2002, 32, 211-216.

78. *JMP*, 10.0.2; SAS Institute Inc.: Cary, NC, 1989-2012.

79. Wiesener, K.; Ohms, D.; Neumann, V.; Franke, R., N_4 Macrocycles as electrocatalysts for the cathodic reduction of oxygen. *Materials Chemistry and Physics* 1989, 22, 457-475.

80. Jaouen, F.; Marcotte, S.; Dodelet, J.-P.; Lindbergh, G., Oxygen reduction catalysts for polymer electrolyte fuel cells from the pyrolysis of iron acetate adsorbed on various carbon supports. *Journal of Physical Chemistry B* 2003, 107, 1376-1386.

81. Charreteur, F.; Ruggeri, S.; Jaouen, F.; Dodelet, J. P., Increasing the activity of Fe/N/C catalysts in PEM fuel cell cathodes using carbon blacks with a high-disordered carbon content. *Electrochimica Acta* 2008, 53, 6881-6889.

82. Rathman, J. In *"Optimal Design" Approaches to DOX*, CHBE 779: "Experimental Design", The Ohio State University, The Ohio State University, 2011.